IEEE Access
Multidisciplinary | Rapid Review | Open Access Journal

Received April 8, 2021, accepted May 2, 2021, date of publication May 7, 2021, date of current version May 17, 2021.

Digital Object Identifier 10.1109/ACCESS.2021.3078194

Speed Control for SRM Drive System Based on Switching Variable Proportional Desaturation PI Regulator

ZIHAN WEI, MI ZHAO, XIMU LIU, AND MIN LU
College of Mechanical and Electrical Engineering, Shihezi University, Shihezi 832003, China
Corresponding author: Mi Zhao (zhaomi530@163.com)

This work was supported in part by the National Natural Science Foundation of China under Grant 61563045, and in part by the International Cooperation Projects of Shihezi University under Grant GJHZ202003.

ABSTRACT This paper develops a novel switching variable proportional desaturation proportional integral (SVPDPI) regulator for speed control of switched reluctance motor (SRM) drive system. Firstly, the idea of desaturation is adopted in the SRM drive system in order to eliminate the integral saturation phenomenon of traditional proportional integral (PI) regulator. Secondly, the variable proportional desaturation PI (VPDPI) regulator is proposed to enhance the response speed of SRM drive system by introducing the concept of variable proportion. In addition, in order to improve the smoothness of the SRM start-up speed, a switching speed regulator is further designed based on the VPDPI regulator. Finally, the principle of error threshold segmentation is introduced into SVPDPI regulator, whose control performance is compared with among other three regulators under rated speed, various speeds and load-torque conditions. Meanwhile, the dynamic performance, steady performance and start-up performance are comprehensively analyzed. The simulation experiment results commendably indicate that the proposed SVPDPI regulator is superior in tracking performance, anti-disturbance performance and speed range.

INDEX TERMS SRM, switching speed regulator, integral desaturation, variable proportional control, speed jitter suppression.

I. INTRODUCTION

With the increasingly stringent global demand for energy conservation, the applications of electric drive in transportation, industry, agriculture and other fields are gradually increasing [1]–[4]. As the core component of the electric drive system, the control of the motor has gradually become a paramount research direction [5]–[7]. Compared with other types of motors, switched reluctance motor (SRM) is usually characterized by flexible control, simple structure, low cost and high efficiency [8]–[10]. There is no winding or permanent magnet on the rotor of the SRM, which increases the reliability of the electrical drive system under high speed and high temperature operating conditions, and economizes the cost of motor manufacturing [8], [11]. Meanwhile, since the unique double-salient pole structure of SRM, when any winding or phase of the motor fails, the stable operation of the SRM drive system can be guaranteed, which provides a favorable advantage for the wide application of the SRM drive system [12]–[14]. At present, one of the most concern in SRM drive system is how to optimize the dynamic quality of speed regulation, especially in star-up stage.

In order to realize more ideal driving performance in SRM, the advanced control mechanism is increasing favored by most scholars to improve the speed response effect of SRM driving system, which can be usually achieved by two ways. The first type is to develop the intelligent controller, such as fuzzy control [15]–[17], slide mode control [18], [19], adaptive control, and artificial neural network [20]–[22]. Obviously, those intelligent algorithms require the complicated procedures and expert users in the design stage, which is limited for its industrial application. Furthermore, another one is optimization approaches, for instance ant colony algorithm, particle swarm optimization algorithm and other optimization algorithms [23]–[26], which take specific speed response performance index as the optimization target,

The associate editor coordinating the review of this manuscript and approving it for publication was Zhuang Xu.

establishes constraint conditions, and then improve the specific speed response performance of the driving system. However, there is no doubt that the control process of the optimization algorithms require a large amount of computation and data processing, which puts forward a higher demand for the arithmetic capability of the controller in the practical application.

Nowadays, it cannot be denied that PI controller is still popular in industries in spite of the remarkable achievements on intelligent control technique, which is because the PI controller has a simple structure, convenient operation, high reliability and cost-effective. In addition, easily modeling, lower user-skill requirement and development complexity bring it to more suitable for engineering practice than those advanced control methods. As mentioned above, the traditional PI regulators are used to achieve the speed control of SRM drives [27]. Unfortunately, the traditional PI control cannot satisfy the actual requirements as the nonlinear factors, external disturbances and the variation of internal parameters intensifies, which leads to its application is greatly restricted. One of the major factors is the existence of the integral saturation [28], [29]. To address this, some scholars adopt the idea of anti-saturation in motor control system such that the saturation phenomenon can be resisted [30]–[33]. Actually, it can realize the suppression of integral saturation to a certain extent. However, it is necessary to point out that the steady-state error could be generated in the speed regulation system if the threshold setting is not reasonable. Hence, the behavior of passive resistance cannot solve the issue fundamentally. By contrast, the desaturation methods perform better steady-state performance than that of the anti-saturation regulator [34], [35]. However, on the downside, its dynamic quality of the speed control system is not fine. Consequently, how to take into account both the dynamic performance and the steady-state one is vital for improving the PI controller.

Motivated by above discussion, this paper propose a novel switching PI control method by combining the desaturation principle and variable proportional method. On one hand, the desaturation idea is adopted to design SRM speed regulator such that the stability of motor control system is improved. On the other hand, the idea of variable proportional desaturation is proposed to achieve better dynamic and steady performance in order to improve the dynamic performance of the regulator. In addition, in order to improve the chattering of the motor in the starting stage, the control algorithm is further improved in this paper, and a design idea of a switch-proportional desaturation regulator is proposed to ensure the speed, accuracy and stability of the switched reluctance motor drive system in the starting stage and the response process.

The rest of this paper is organized as follows. Section II presents the mathematical model of the three-phase SRM. Three improved PI speed regulators are designed in Section III after revealing the drawbacks of traditional PI controller. In Section IV, the proposed speed regulators are simulated and verified on SRM drive system, whose performance analysis is also carried out by comparing the traditional PI regulator. Finally, Section V concludes the article.

II. THE MATHEMATICAL MODEL OF THREE-PHASE SRM

Taking the three-phase SRM as a control object, this section proposes its mathematical model. In details, the relationship between the speed and the motor parameters is established based on its electromechanical relation equation. In order to simplify the model analysis process, the following assumptions are proposed:

Assumption 1: The inductance is equivalent to a linear model.

Assumption 2: The viscosity coefficient of the system is ignored.

Based on the above assumptions and references [36], [37], the equivalent inductance model is depicted as (1):

$$L(\theta) = \psi_m(a + b\sin(N_r\theta)) \tag{1}$$

Furthermore, its electromagnetic torque can be simplified to an univariate function of position angle when the current is given, which can be derived as follows:

$$T_e = \frac{1}{2}i^2\frac{dL}{d\theta} = \frac{1}{2}i^2(bN_r\psi_m\cos(N_r\theta)) \tag{2}$$

where ψ_m and θ denote the flux saturation value and position angle, respectively. In addition, a and b are both undetermined coefficients, which can be calculated through obtaining the motor parameters. N_r represent the number of rotor poles.

Therefore, its motion equation can be constructed in terms of the law of the fixed-axis rotation [38].

$$\frac{d\omega}{dt} = \frac{1}{J}(T_e - T_L) = \frac{1}{J}(\frac{1}{2}i^2bN_r\psi_m\cos(N_r\theta) - T_L) \tag{3}$$

where ω and J are the motor rotation angular velocity and instantaneous value of inertia, respectively, and T_L denotes the load torque.

According to the Kirchhoff's voltage law (*KVL*), the voltage equation of SRM is deduced based on its equivalent armature circuit [39], which is shown in (4):

$$u - iR_s = L\frac{di}{dt} + i\frac{dL}{d\theta}\frac{d\theta}{dt} \tag{4}$$

where u is DC voltage, and R_s is stator resistance. By combining (1) with (4), the first-order differential equation of the phase current can be obtained as shown in (5):

$$\frac{di}{dt} = \frac{u - iR_s - i\omega bN_r\psi_m\cos(N_r\theta)}{\psi_m(a + b\sin(N_r\theta))} \tag{5}$$

Assuming that the speed is constant, equation (5) is further simplified as follows:

$$i = \frac{u}{\omega bN_r\psi_m\frac{\int_0^T\cos(N_r\theta)dt}{T}} \tag{6}$$

After that, equation (6) is substituted into (3), then we have the following equation:

$$\frac{d\omega}{dt} = \frac{1}{J}(\frac{1}{2}\frac{u^2}{\omega^2bN_r\psi_m\frac{\int_0^T\cos(N_r\theta)dt}{T}} - T_L) \tag{7}$$

Finally, the motion equation of SRM is obtained as shown in (7). When the SRM operates in the steady state, the speed variation rate tends to zero, whose average speed $\overline{\omega}$ is written as follows:

$$\overline{\omega} = \sqrt{\frac{\overline{u^2}}{2T_L bN_r \psi_m \frac{\int_0^T \cos(N_r\theta)dt}{T}}} \tag{8}$$

After that, equation (7) is discretized at $(\overline{\omega}, \overline{u})$ by utilizing the infinitesimal method, and then the speed regulation ratio is deduced as follows:

$$\frac{d\omega}{dt} = \frac{d\alpha}{dU}|_{\overline{\omega},\overline{u}}\Delta u + \frac{d\alpha}{d\omega}|_{\overline{\omega},\overline{u}}\Delta\omega \tag{9}$$

After the Laplace transform, the transfer function of control voltage and speed is derived as shown in (10):

$$\begin{aligned}\frac{\Delta\omega(s)}{\Delta u(s)} &= \frac{\frac{2T_L}{J\overline{u}}}{s + \frac{2T_L}{J\overline{u}}\sqrt{2T_L bN_r\psi_m\frac{\int_0^T\cos(N_r\theta)dt}{T}}} \\ &= \frac{\frac{\overline{\omega}}{\overline{u}}}{JbN_r\psi_m\overline{cos(N_r\theta)}\frac{\overline{\omega^3}}{\overline{u^2}}s+1} = \frac{k_p}{sT_p+1}\end{aligned} \tag{10}$$

where, $k_p = \frac{\overline{\omega}}{\overline{u}}$, $T_p = JbN_r\psi_m\overline{cos(N_r\theta)}\,\frac{\overline{\omega^3}}{\overline{u^2}}$.

Based on the above theoretical deduction, the mathematical model of a three-phase SRM is established. Subsequently, the speed regulator of SRM drives and its related parameters would be designed and specified.

III. DESIGN OF SPEED REGULATORS

There is no doubt that the speed control performance is determined by its speed regulator. At present, the traditional PI regulator is difficult to achieve the high precision motion control due to its undesirable dynamic quality and out of control. To achieve this, a novel controller and its related control algorithm are proposed by analyzing the deficiency of design philosophy in the traditional PI regulator.

A. THE CHARACTER OF CONVENTIONAL PI SPEED REGULATOR

In the speed regulating system [16], [40], the input signal of the speed regulator is the speed error signal e, and whose output signal is the system reference torque, which is denoted as $u(t)$. Based on the traditional PI control, its control rule is described as Eq. (11).

$$u(t) = K_p e + K_i \int edt \tag{11}$$

where K_p (resp. K_i) is the proportional coefficient (resp. integral coefficient). However, when the integral link accumulates to a certain extent, the regulator will saturate. From the point of view of the control principle, the phenomenon of integral saturation is easy to cause the large overshoot of the speed n. Meanwhile, the stability of the output signal T^* of the regulator is greatly affected.

In order to suppress the action time of integral saturation in the control system, the references in [30]–[33], [35] adopt the idea of anti-saturation to improve the comprehensive performance of the speed control system. When the regulator entered the saturation state, the effect of integral element is removed. This method can resist the integral saturation phenomenon and improve the dynamic response performance of the system. However, the saturation state cannot be completely eliminated. Meanwhile, the steady state error cannot be avoided since the poor regulation mode of proportional element is only left. Hence, how to eliminate the influence of integral saturation in essence is worthwhile without sacrificing the steady-state performance of the system.

B. A NOVEL DESIGN OF SVPDPI SPEED REGULATOR FOR SRM DRIVE SYSTEM

In order to obtain the better regulation performance in the SRM drive system, the above issues of traditional PI control are well addressed in this paper. Subsequently, three advanced regulators and their related control principles are presented gradually in the following subsections.

1) DPI SPEED REGULATOR

Through the research and analysis of anti-saturation technology, this paper puts forward an improvement measure of de-saturation PI type (DPI) based on the SRM motor speed regulation system. When the phenomenon of integral saturation occurs, DPI attenuates the integral saturation accumulation by introducing the feedback compensation coefficient γ, whose structural block diagram of the DPI control method is shown in Fig. 1.

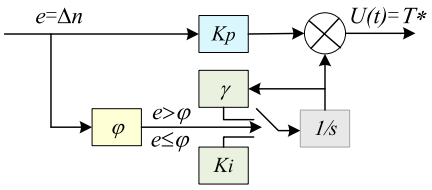

FIGURE 1. The structure diagram of DPI regulator control algorithm.

According to the control law of the DPI control algorithm, the governing equation is derived as Eq. (12):

$$u(t) = K_p e + \gamma K_i \int edt \tag{12}$$

In Eq. (12), φ is the threshold used to determine whether to introduce the compensation coefficient. And if $e > \varphi, \gamma < 0$ otherwise $\gamma = 1$.

2) VPDPI SPEED REGULATOR

Obviously, the stead-state error can be eliminated by utilizing the DPI regulator according to (12). However, the response speed of this algorithm has still certain limitations. In order to improve the dynamic performance of the regulator, an improved method of variable proportional desaturation PI (VPDPI) regulator is proposed in this subsection. From the

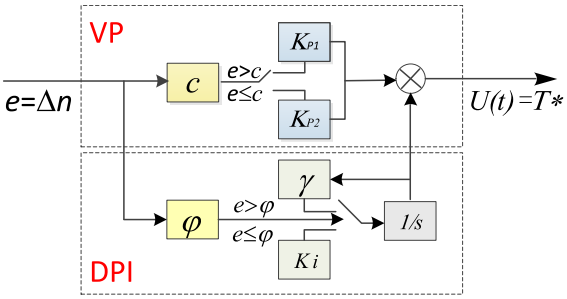

FIGURE 2. The structure diagram of VPDPI regulator control algorithm .

control principle, it is clearly that the dynamic and steady-state performance of the controlled system are both improved due to the fast response of proportional element. The corresponding control block diagram of the VPDPI algorithm is shown in Fig. 2.

From Fig. 2, the VPDPI controller can be mainly divided into two sub-controllers, that is the variable proportion part and the desaturation part. The algorithm selects the appropriate proportional coefficient by judging the size of the rotational speed error signal e, and decides whether to introduce the feedback compensation coefficient γ. The control law of the VPDPI algorithm is shown in Eq. (13).

$$u(t) = [\rho(K_{p2} - K_{p1}) + K_{p1}]e + \gamma K_i \int edt \tag{13}$$

In (13), let ρ be the selection coefficient, and if $e > c$ (c is the threshold used to determine whether to change the proportionality coefficient) then $\rho = 0$, otherwise $\rho = 1$.

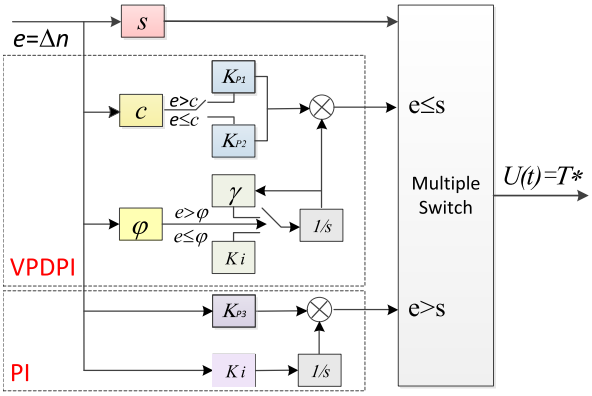

FIGURE 3. The structure diagram of SVPDPI regulator control algorithm.

3) SVPDPI SPEED REGULATOR

Although VPDPI algorithm can improve the dynamic response in some extent compared with DPI regulator, it cannot be denied that it is easy to aggravate the speed instability and oscillation phenomenon accompanied by the proportional coefficient mutates. Secondly, the jitter of rotation speed can lead to the adverse impact on the equipment during the motor startup stage. Based above consideration, this subsection proposes the switched variable proportional and desaturation PI (SVPDPI) algorithm, whose corresponding structural block diagram is shown in Fig. 3. And the governing equation is derived as (14):

$$\begin{cases} u(t) = [\rho(K_{p2} - K_{p1}) + K_{p1}]e + \gamma K_i \int edt \ (e \le s) \\ u(t) = K_{p3}e + K_i \int edt \ (e > s) \end{cases} \tag{14}$$

According to the structure block diagram of the control algorithm, the concrete implementation steps are shown in Algorithm 1.

Algorithm 1 The Computation Algorithm of *SVPDPI* for SRM Drive System

Input: The given speed of SRM drive system n_N^*
Output: The referenced torque T_e^*

```
begin;
Setting n_N^*, s
Identify and Sampling n at t time.
Calculating the error value of speed e = n_N^* − n
if e ≤ s then
    u(t) = [ρ(K_p2 − K_p1) + K_p1]e + γK_i ∫ edt
else
    u(t) = K_p3 e + K_i ∫ edt
end if
Output u(t), where u(t) is the referenced torque T_e^* at t moment.
end.
```

It is worth noting that the equivalent transfer function $W_{SRM}(s)$ of the speed regulating system has been obtained in Eq. (10), which can be superposition with the proposed SVPDPI algorithm as the transfer function by the control principle, and the equation of its coefficient can be obtained in Eq. (15).

In general, the errors of equivalent parameters cannot be completely avoided due to the approximate equivalence in the mathematical model. Hence, the modified coefficients (K_a, K_b) of the regulator are adopted to weaken the principal error such that it facilitate the parameters debugging in SRM drive system.

$$\begin{cases} K_{p_i} = \dfrac{K_a}{k_p} = K_a \dfrac{\overline{u}}{\overline{\omega}} \ (i = 1, 2, 3) \\ K_i = \dfrac{1}{T_p} = K_b \dfrac{\overline{u^2}}{\overline{\omega^3}} \end{cases} \tag{15}$$

Remark 1 (A Select Principle of Threshold φ and Feedback Compensation Coefficient γ): The feedback compensation coefficient γ ($\gamma < 0$) can eliminate integral saturation by reverse accumulation error Δn. A larger $|\gamma|$ will weaken the effect of the regulator integral link, thus the drive system will exist the steady-state error. However, a smaller $|\gamma|$ will make the system exist a certain amount of overshoot due to incomplete desaturation. The influence of different feedback compensation coefficients on the driving system is shown in Appendix A.

On the other hand, the desaturation effect of the system is closely related to the action time of the feedback compensation coefficient γ. According to the relationship between the threshold φ and the speed error Δn, the desaturation link can automatically judge whether the feedback compensation coefficient need is introduced or not. When the speed error Δn exceeds the threshold φ, the feedback compensation coefficient starts to act until the error is within the threshold. The effects of different thresholds on the driving system are shown in Appendix B.

From the perspective of the simulation experiment, the influence of the value of the feedback compensation coefficient γ and the action time on the driving system are verified by the waveforms in Appendix A and B, respectively. A selection rule is established for parameter setting of feedback compensation coefficient γ and threshold φ of different driving systems.

Remark 2 (A Select Principle of Threshold c and Coefficient ρ): Selection coefficient ρ is similar to a switch signal. The switch states closely related to the threshold c. When the speed error Δn is greater than the threshold value c, then $\rho = 1$, it enters the variable proportion link. Otherwise, it is the traditional control mode. The effects of different thresholds on the driving system are shown in Appendix C.

Appendix C reveals that excessive threshold c will increase the response speed. Unfortunately, the risk of system jitter is also strengthened at the same time. Therefore, a reasonable selection should be made according to the actual control requirements. In summary, both γ and ρ aim to improve the system dynamics without changing the steady-state performance of the drive system.

Remark 3 (A Select Principle of Threshold s): In order to improve the rapid response performance of the system and ensure the stability of the system, an ''insurance'' is added to the system through the threshold s. When the speed error Δn exceeds the threshold s, the traditional PI regulator is used as the speed regulator. On the contrary, the VPDPI regulator acts on the drive system. Generally, the threshold s should be less than the threshold c since the sudden addition of the variable proportion link, which can easily lead to the temporary jitter of the system. The effects of different thresholds on the driving system are shown in Appendix D.

Actually, the influence of different threshold s values on the driving system has also been briefly proved in the simulation diagram. The trend of the two groups of waveforms is basically the same when the threshold s is less than the threshold c. However, the waveform whose threshold s is greater than the threshold c obviously reflects the action time of the variable proportion link. If the variable proportion parameter is not selected properly, the system may still have the problem of temporary jitter.

C. THE SPEED REGULATOR STABILITY VERIFICATION

Based on the SVPDPI regulator design in Section III-B3, the system dynamics can be obviously improved by introducing the coefficient γ and ρ without destroying the stability of the traditional PI. Hence, this subsection will further verify the stability of the drive system based on the traditional PI regulator. According to the transfer function in (10) and the PI regulator control rule in (11), the open loop transfer function of the drive system is obtained as follows:

$$G(s) = W_{SRM}(s) \times W_{PI}(s) = \frac{k_p \cdot k_c \cdot s + k_i \cdot k_p}{T_p \cdot s^2 + s} \quad (16)$$

where k_c and k_i are defined as the proportionality coefficient and the integration coefficient of the PI regulator, respectively.

The transfer function of the closed-loop system is obtained by using the Mason gain formula as follows:

$$\Phi(s) = \frac{G(s)}{1 + G(s)} = \frac{k_p \cdot k_c \cdot s + k_i \cdot k_p}{T_p \cdot s^2 + (1 + k_p \cdot k_c)s + k_i \cdot k_p} \quad (17)$$

Substitute the data in Table 1 into (10) to get $T_p = 5.104$, and $K_p = 8.727$. Therefore, equation (17) is transformed into:

$$\Phi(s) = \frac{8.727k_c \cdot s + 8.727k_i}{5.104s^2 + (1 + 8.727k_c)s + 8.727k_i} \quad (18)$$

Set the driving system characteristic polynomial $D(s)$ as:

$$D(s) = 5.104s^2 + (1 + 8.727k_c)s + 8.727k_i \quad (19)$$

According to Routh criterion, the condition of system stability is:

$$\begin{cases} 1 + 8.727k_c > 0 \\ k_i > 0 \end{cases} \quad (20)$$

The solution of (20) is as follows:

$$\begin{cases} k_c > -0.121 \\ k_i > 0 \end{cases} \quad (21)$$

IV. THE SIMULATION ANALYSIS AND PERFORMANCE COMPARASION

A. THE OVERALL STRUCTURE AND PARAMETER SETTINGS OF THE SRM DRIVE SYSTEM

1) THE OVERALL STRUCTURE OF THE SRM DRIVE SYSTEM

In this article, the SRM drive system employs the control structure of direct torque control (DTC), whose structure is usually composed of the double closed-loop mode. The inner loop includes the torque and flux loops through the direct torque controller. Among them, the actual torque T is the torque output by the SRM. In addition, the total flux ψ_s and flux angle θ_s are obtained from the phase flux output by the SRM through the flux calculation link. The outer loop is primary feedback, which achieves the speed control by the proposed speed regulator. The structure block diagram of the whole controlled system is shown in Fig. 4. Furthermore, the simulation model of SRM drive system based on the proposed speed regulator is further constructed based on the MATLAB/Simulink platform.

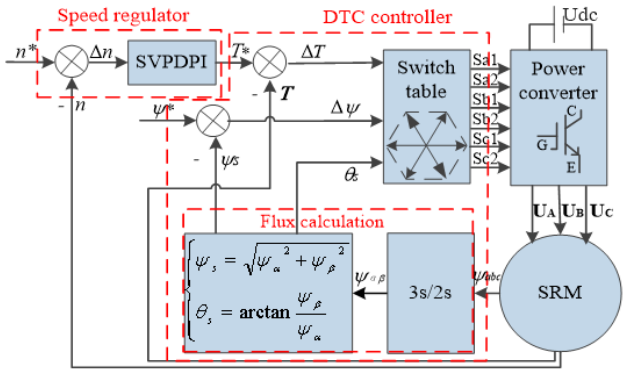

FIGURE 4. The SRM drive system structure block diagram.

TABLE 1. The rated parameters of the SRM.

Symbol	Parameters	Value
P_N	Rated power	60 kW
$n*$	Rated speed	1000 rpm(r/min)
$\psi*$	Rated flux link	0.28 Wb
U_{dc}	DC voltage	240 V
J	Inertia	0.05 kg.m^2
L_d	Aligned inductance	0.67 $\times 10^{-3}$ H
L_q	Unaligned inductance	23.62 $\times 10^{-3}$ H
L_m	Saturation inductance	0.15 $\times$ 10^{-3} H
R_s	Stator resistance	0.05 Ω
B	Friction coefficient	0.02 N·m· s

TABLE 2. The main parameters of SRM drive system model.

Parameters	Value	Parameters	Value
K_{p1}	0.1	K_{p2}	1
K_{p3}	0.023	K_i	0.1
γ	-14	s	50
c	230	φ	100

2) PARAMETER SETTINGS OF THE SRM DRIVE SYSTEM

The rated parameters of the SRM in the simulation process are shown in Table 1.

In addition, in order to verify the control performance of the proposed speed regulator, the regulator parameters mentioned in section III are set as shown in Table 2.

B. SIMULATION AND COMPARISON BASED ON DIFFERENT SPEED REGULATORS

In Section I, it has been mentioned that the tracking performance, anti-disturbance performance and the speed range are important basis for measuring the performance of the SRM drive system. Therefore, this section would be divided into four parts to carry out simulation verification of the proposed regulators.

This section firstly simulates the running state of the SRM at rated speed, and obtains the tracking quality of the SVPDPI regulator by analyzing the dynamic and steady performance of the speed response under a variety of regulators. Secondly, it is necessary to analyze the dynamic tracking performance of the controlled system under the condition of speed fluctuation such that the anti-speed disturbance ability of the proposed regulators is verified. Furthermore, in order to comprehensively verify the resistance ability of SVPDPI regulator to load torque disturbance, the dynamic fall and recovery times of the speed response curve under load mutation are compared and analyzed, and the load disturbance ability of SVPDPI regulator is summarized. Finally, taking the stability of the response curve as the standard, the differences between the proposed regulators and the traditional PI regulator in the speed adjustment range are compared and analyzed. Finally, taking the stability of the response curve as the standard, the differences between the proposed regulator and the traditional PI regulator in the speed adjustment range are compared and analyzed.

1) THE CONTROL PERFORMANCE ANALYSIS OF SVPDPI REGULATOR AT RATED SPEED

Initially, the proportion and integration coefficients of the traditional PI regulator are exactly the same as that of the SVPDPI regulator. When the SRM runs at the rated speed ($n = 1000\ rpm$), the waveform of speed control effect of four regulators within $t = 0$ second to $t = 1$ seconds based on the same parameter setting are shown in Fig. 5.

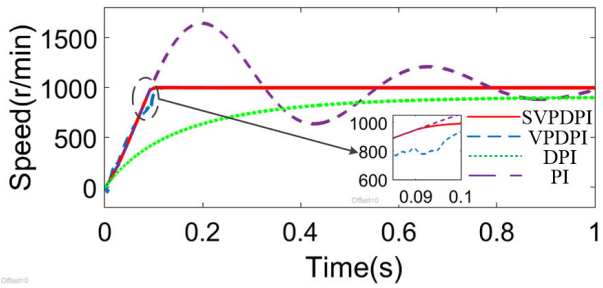

FIGURE 5. The waveform diagram of SVPDPI regulator control effect at rated speed.

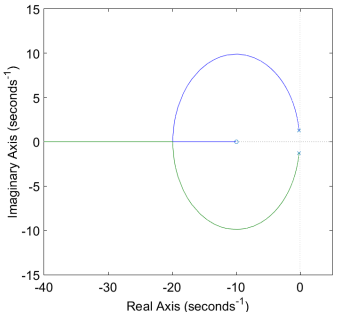

FIGURE 6. The root locus of the SRM drive system.

It is well known that stability, accuracy, rapidity and smoothness are important performance indicators to measure the drive system. Obviously, the stability is the primary performance of the system. In order to verify the stability of the system, the parameters in Table 2 are substituted into (20) to obtain the drive system closed-loop root locus as shown in Fig. 6:

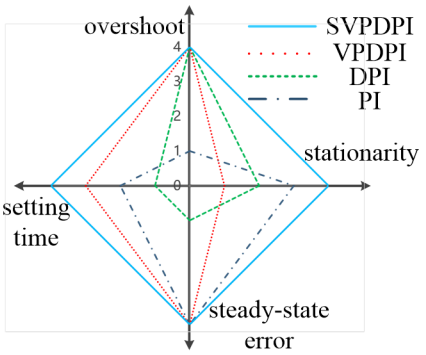

FIGURE 7. The radar chart of performance comparison of four regulators at rated speed.

It is clearly from the root locus that all locus are located in the left half plane, which proves that the system based on the parameters used in this paper is stable.

In order to intuitively compare the other performance of various regulators at rated speed, the comprehensive evaluation scheme of various speed regulators is obtained according to the simulation results, as shown in Fig. 7. If the regulator has a higher score in the radar chart, which is consided that the regulator has a better control performance.

According to Fig. 5 and Fig. 7, the DPI regulator can eliminate the large overshoot of the traditional PI regulator by approximately 65 %. However, its response speed is significantly reduced, which leads to the slow recovery time of the traditional PI regulator. Meanwhile, there is a weak speed jitter at the beginning of the start-up stage. The response speed of the DPI regulator is improved based on the variable proportion action in the VPDPI regulator. Nevertheless, it also intensifies the unstable of the speed at the start-up stage of the SRM when the variable proportion link is applied. However, the SVPDPI regulator combines the advantages of PI and VPDPI. On one hand, the overshot of the speed response curve is eliminated. On the other hand, the response speed and stationarity of the system are both improved.

Notation 1: In Fig. 5, it should be noted that the dynamic performance of the traditional PI controller maybe not ideal, particularly in overshoot, whose foundational reason lies in improper control parameters. Certainly, it can be further improved along with the adjustment of K_p and K_i. However, the optimal parameters always require continuous debugging or professional experience, especially in the situation of variable structure or operation condition, which leads to high computation load. By contrast, the proposed method can achieve the self-align of control parameters by utilizing the concept of error threshold even though the conventional PI parameters is undesirable, which can avoid complex processing. The comparison results also indicate that the proposed method can achieve more better performance than the traditional PI controller under the same control parameters.

The waveform diagram of total flux, torque and current control effect of SVPDPI regulator are shown in Figs. 8-10, respectively.

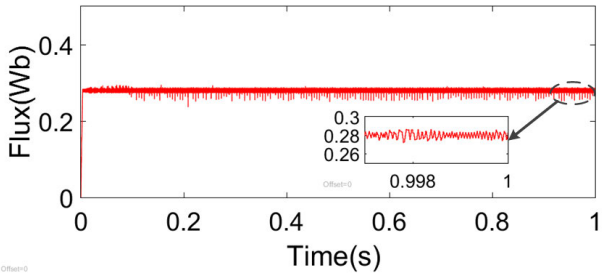

FIGURE 8. The waveform diagram of flux control effect of SVPDPI regulator at rated speed.

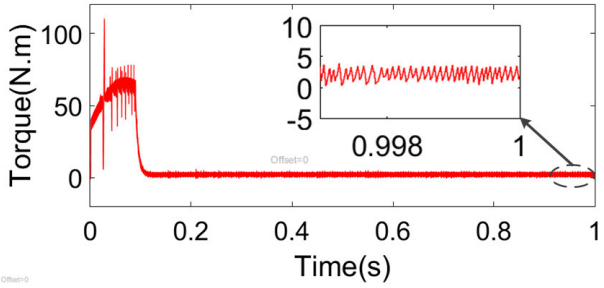

FIGURE 9. The waveform diagram of torque control effect of SVPDPI regulator at rated speed.

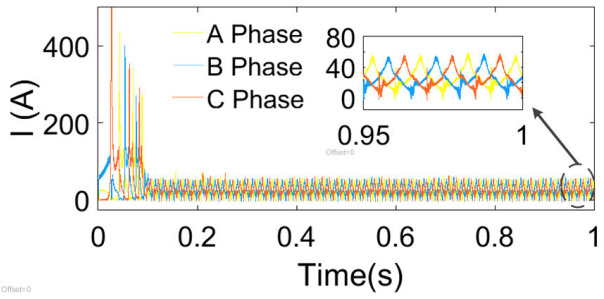

FIGURE 10. The waveform diagram of current control effect of SVPDPI regulator at rated speed.

Above all, DPI has certain advantages in eliminating system overshoot, while VPDPI has outstanding effects in improving system response speed and eliminating system overshoot. In addition, compared with the other three regulators, SVPDPI regulator improves the comprehensive speed control ability of SRM drive system on the basis of guaranteeing the ideal control of flux linkage, torque and current.

2) THE CONTROL PERFORMANCE ANALYSIS OF SVPDPI REGULATOR UNDER SPEED DISTURBANCE

The SVPDPI controller has been verified to have better speed regulation performance under ideal starting conditions. However, there is usually a disturbance at actual run operation. Therefore, it is necessary to verify if the proposed method gives satisfactory control performance even in speed and load torque variation condition. Firstly, the operational performance of SRM is simulated under the variable speed.

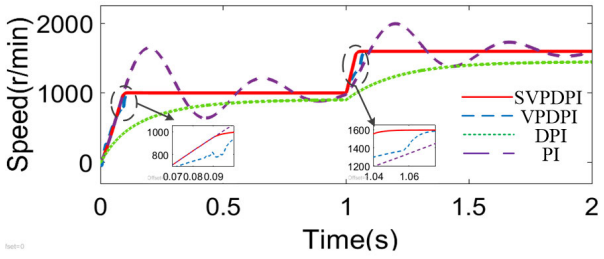

FIGURE 11. The waveform of speed with speed disturbance.

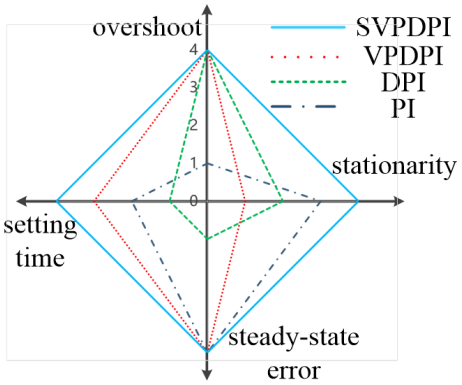

FIGURE 12. The radar chart of performance comparison of four regulators with speed disturbance.

The initial speed is set as 1000 *rpm*, and then it breaks to 1600 *rpm* at 1 seconds. Fig. 11 illustrates the comparison waveform of the speed response curve of the four regulators within $t = 0$ to $t = 2$ seconds.

To visually compare the ability of various regulators to resist speed disturbances, the comprehensive analysis results obtained according to the simulation results are shown in Fig. 12. According to Fig. 11 and Fig. 12, the SVPDPI regulator can quickly track the new given speed at the sudden change of speed in the SRM drive system, and the dynamic process is stable without overshoot. Compared with SVPDPI controller, VPDPI controller and DPI controller have unfavorable performance in response process stability and response speed. The traditional PI regulator not only has a slow response speed, but also has a large overshoot, which fails to achieve ideal dynamic and steady-state performance.

The waveform diagram of total flux, torque and current control effect of SVPDPI regulator are shown in Figs. 13-15, respectively.

It can be seen from the waveform and radar map that the SVPDPI regulator returns to a stable state faster and more smoothly after a short speed change compared to other types of regulator. Meanwhile, the SRM torque, flux and current values are quickly restored to a stable range. The integrated speed control performance of SVPDPI regulator is significantly improved than other regulators.

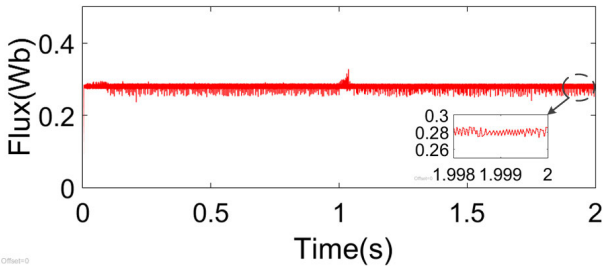

FIGURE 13. The waveform of flux control effect of SVPDPI regulator with speed disturbance.

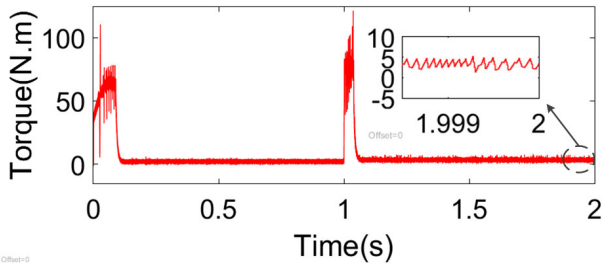

FIGURE 14. The waveform of torque control effect of SVPDPI regulator with speed disturbance.

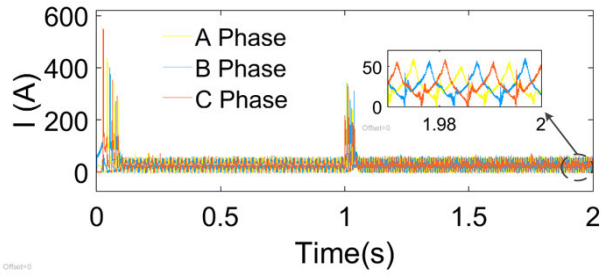

FIGURE 15. The waveform of current control effect of SVPDPI regulator with speed disturbance.

3) THE CONTROL PERFORMANCE ANALYSIS OF SVPDPI REGULATOR UNDER LOAD DISTURBANCE

The SRM drive system based on SVPDPI regulator has strong resistance to the sudden disturbance of speed. In addition, when the external load changes, the simulation analysis of the SRM drive system is also an important reference to verify the performance of the SVPDPI regulator. Therefore, the system load torque is 5 $N \cdot m$ when $t = 2$ seconds, and it will be doubled after one second. Subsequently, the speed control effect waveform of four regulators can be obtained as shown in Fig. 16.

According to Fig. 16, when the SRM drive system is suddenly applied a various load torque, the dynamic descent of the SRM drive system based on traditional PI regulator is obvious. Compared with the control effect of traditional PI regulator, the drive system based on DPI regulator appears bigger dynamic drop, and the recovery time is longer.

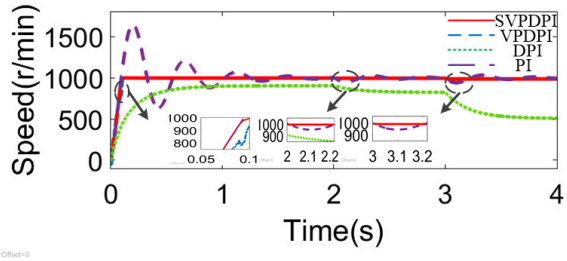

FIGURE 16. The speed control effect waveform of SVPDPI regulator with variable load torque.

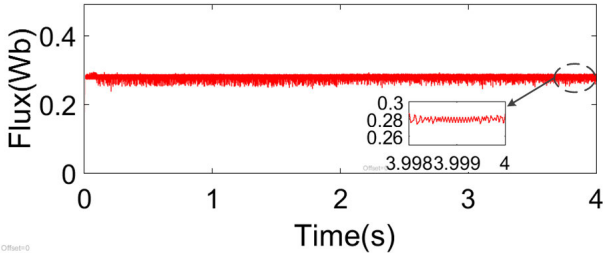

FIGURE 17. The flux control effect waveform of SVPDPI regulator with variable load torque.

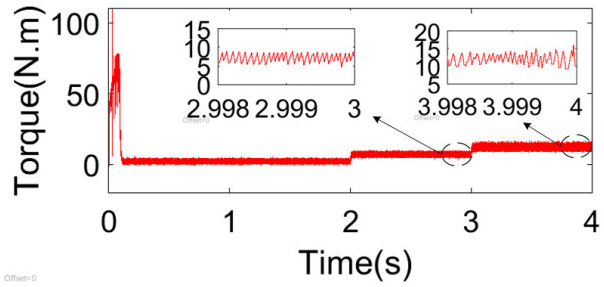

FIGURE 18. The torque control effect waveform of SVPDPI regulator with variable load torque.

Compared with the above two regulator control effects, the speed regulation system based on SVPDPI and VPDPI regulator control are less dynamic landing, and the recovery time is more faster. The control performance of the four regulators at $T_L = 5\ N \cdot m$ is absolutely consistent with that at $T_L = 10\ N \cdot m$. This also explains the consistency of the regulator's control performance under low and high load perturbations.

The waveform diagram of total flux, torque and current control effect of SVPDPI regulator are shown in Figs. 17-19, respectively.

Obviously, the control effect of stator flux is not affected during the disturbance of load torque, as shown in Fig. 17. The torque response curve in Fig. 18 also reveals the dynamic variation of electromagnetic torque in matching the load torque. Undoubtedly, DTC plays an irreplaceable role in independently control for the torque and flux. Moreover, stator phase current is weakly increased during the loading period, as shown in Fig. 19. However, the high overshoots are not

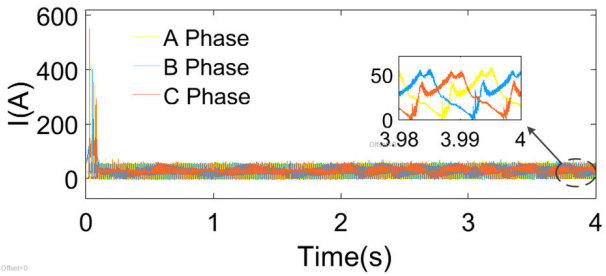

FIGURE 19. The current control effect waveform of SVPDPI regulator with variable load torque.

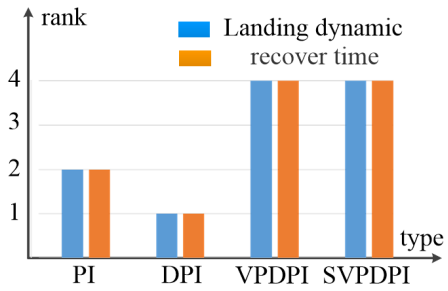

FIGURE 20. The comparison of four regulators with variable load torque.

detected during the transient period, which means that the current is properly controlled except during the starting stage.

In order to visually compare the ability of four regulators to resist various load disturbances, the recover time and landing dynamic performance analysis of the four regulators are shown in Fig. 20. From the above results, compared with other kinds of regulators, SVPDPI regulator has a higher performance under various load torque conditions. When the external load changes, the total flux linkage, torque and current control of the drive system based on SVPDPI regulator is stable. The various load torque conditions have little influence on the speed control, which verifies the capability of the regulator in resisting load disturbance.

4) THE SPEED CONTROL RANGE OF SRM DRIVE SYSTEM BASED ON SVPDPI REGULATOR

In the previous subsection, the performance of SVPDPI regulator in terms of the control accuracy, fast response and its speed tracking and anti-load variation capabilities has been verified and analyzed. The simulation results reveal that SVPDPI controller provides favorable performance with high speed running (1600 *rpm*). Nevertheless, the operation stability in the low speed circumstance should never be ignored especially in wide speed control system. Therefore, this subsection simulates the operation of the SRM drive system at a low speed to verify the speed adjustment range of different regulators. When the speed is set at 600 *rpm*, whose waveform diagram of speed response is shown in Fig. 21. From Fig. 10, it can be found that the traditional PI regulator generates a large overshoot even out of the control when the

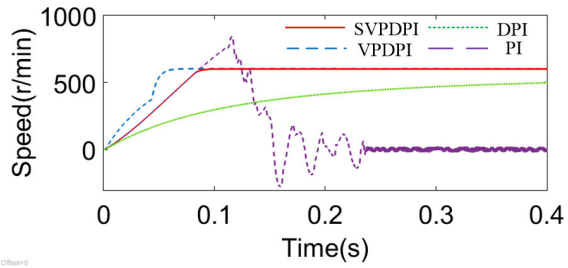

FIGURE 21. The speed control effect waveform diagram at $n = 600$ *rpm*.

given speed is 600 *rpm*. Certainly, the system stability could be ensured in theory if the control parameters are reasonable. While unfortunate, the existence of integral saturation would disable the controller. The reason for this is that the error change ratio maybe too large, resulting in uncorrectable deviation in the long-term. Therefore, the integral saturation should be completely relieved during the ascent stage. Compared with the other three regulators, the SVPDPI regulator in this article can realize fast and stable tracking to the given value within 600 *rpm* to 1600 *rpm*.

V. CONCLUSION

Based on the characteristic analysis of traditional PI regulator, this paper proposes an original SVPDPI regulator for SRM drive system such that the dynamic response quality of the speed regulation is dramatically improved while the integral saturation of PI regulator is totally eliminated. Specifically, the decisive roles of the desaturation and variable proportion are concurrently imposed on the speed regulator that ensures the favourable dynamic property. More importantly, the new switching regulator achieves the speed smooth of the drive system at start-up stage. Meanwhile, the effectiveness of the proposed method is demonstrated and compared by a comprehensive evaluation method, i.e., the simulation waveforms and their corresponding radar chart. Consequently, it can be verified that the proposed speed regulator can not only achieves the tracking quality of high performance, but also improves strong anti-interference ability and a few speed range. In the future work, the promising track is how to promote the self-adaptability and self-learning ability of the PI regulator to improve its dynamic quality in practical SRM drive system.

APPENDIX A
THE SELECTING PROCESS OF FEEDBACK COMPENSATION COEFFICIENT γ

Taking $\gamma = -14$ as the benchmark in this paper, the waveform aims to verify the influence of variable γ value on the driving system.

APPENDIX B
THE SIMULATION DIAGRAM UNDER DIFFERENT THRESHOLDS φ

On the basis of $\varphi = 100$, the influence of different threshold φ on the driving system is verified by waveform .

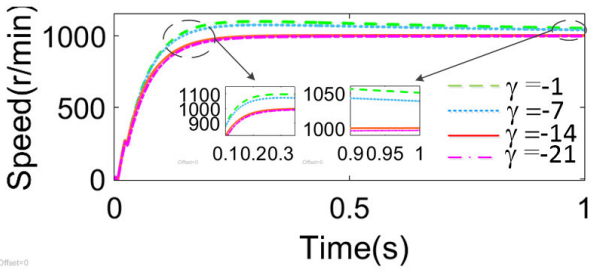

FIGURE 22. The comparison diagram of speed under different feedback compensation coefficients γ.

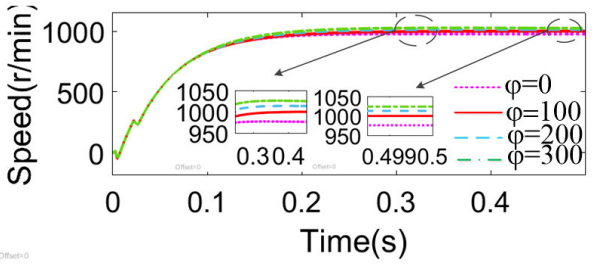

FIGURE 23. The comparison diagram of speed under different thresholds φ.

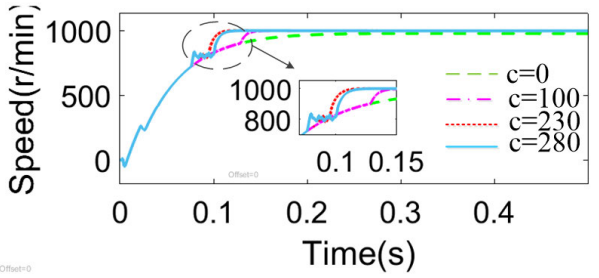

FIGURE 24. The comparison diagram of speed under different thresholds *c*.

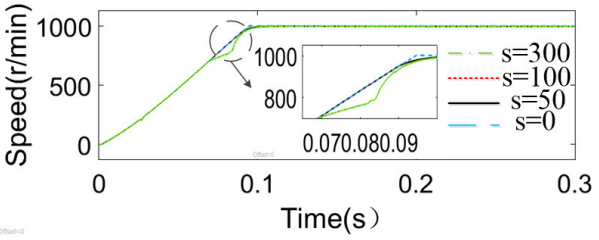

FIGURE 25. The comparison diagram of speed under different thresholds *s*.

APPENDIX C
THE SIMULATION DIAGRAM UNDER DIFFERENT THRESHOLDS *c*

The relationship between different thresholds c and the stability and response speed of the driving system is briefly revealed by the following waveform.

APPENDIX D
THE SIMULATION DIAGRAM UNDER DIFFERENT THRESHOLDS *s*

The following waveform is mainly to verify the control effect of threshold s and threshold c under different relations.

REFERENCES

[1] E. V. Belousov and M. A. Grigorev, "An electric drive for a drilling rig top drive system," *Russian Electr. Eng.*, vol. 91, no. 7, pp. 447–451, Jul. 2020.

[2] D. Liu, S. Huang, S. Wu, and X. Fu, "Direct yaw-moment control of electric vehicle with in-wheel motor drive system," *Int. J. Automot. Technol.*, vol. 21, no. 4, pp. 1013–1028, Aug. 2020.

[3] L. Shao, A. E. H. Karci, D. Tavernini, A. Sorniotti, and M. Cheng, "Design approaches and control strategies for energy-efficient electric machines for electric vehicles—A review," *IEEE Access*, vol. 8, pp. 116900–116913, 2020.

[4] S. Hussain, M. A. Ahmed, and Y.-C. Kim, "Efficient power management algorithm based on fuzzy logic inference for electric vehicles parking lot," *IEEE Access*, vol. 7, pp. 65467–65485, 2019.

[5] J. M. Said, P. Harth, and P. Ficzere, "In-wheel-motor electic vehicles and their associated drivetrains," *Int. J. Traffic Transp. Eng.*, vol. 10, no. 4, pp. 415–431, 2020.

[6] T. Pourseif and M. Mohajeri, "Design of robust control for a motor in electric vehicles," *IET Electr. Syst. Transp.*, vol. 10, no. 1, pp. 68–74, Mar. 2020.

[7] Y. Zhu, H. Wu, and J. Zhang, "Regenerative braking control strategy for electric vehicles based on optimization of switched reluctance generator drive system," *IEEE Access*, vol. 8, pp. 76671–76682, 2020.

[8] C. Gan, J. Wu, Q. Sun, W. Kong, H. Li, and Y. Hu, "A review on machine topologies and control techniques for low-noise switched reluctance motors in electric vehicle applications," *IEEE Access*, vol. 6, pp. 31430–31443, 2018.

[9] K. Vijayakumar, R. Karthikeyan, S. Paramasivam, R. Arumugam, and K. N. Srinivas, "Switched reluctance motor modeling, design, simulation, and analysis: A comprehensive review," *IEEE Trans. Magn.*, vol. 44, no. 12, pp. 4605–4617, Dec. 2008.

[10] M. Zeraoulia, M. E. H. Benbouzid, and D. Diallo, "Electric motor drive selection issues for HEV propulsion systems: A comparative study," *IEEE Trans. Veh. Technol.*, vol. 55, no. 6, pp. 1756–1764, Nov. 2006.

[11] P. Sovicka, P. Rafajdus, and V. Vavrus, "Switched reluctance motor drive with low-speed performance improvement," *Electr. Eng.*, vol. 102, no. 1, pp. 27–41, Mar. 2020.

[12] S. Xu, H. Chen, and F. Dong, "Converter-level reliability prediction and analysis in switched reluctance motor drive," *IET Electr. Power Appl.*, vol. 14, no. 3, pp. 500–511, Mar. 2020.

[13] Y. Hu, C. Gan, W. Cao, J. Zhang, W. Li, and S. J. Finney, "Flexible fault-tolerant topology for switched reluctance motor drives," *IEEE Trans. Power Electron.*, vol. 31, no. 6, pp. 4654–4668, Jun. 2016.

[14] C. Gan, J. H. Wu, S. Yang, W. Cao, J. L. Kirtley, and Y. H. Hu, "Online sensorless position estimation for switched reluctance motors using one current sensor," *IEEE Trans. Power Electron.*, vol. 31, no. 10, pp. 7248–7263, Oct. 2016.

[15] S. Bolognani and M. Zigliotto, "Fuzzy logic control of a switched reluctance motor drive," *IEEE Trans. Ind. Appl.*, vol. 32, no. 5, pp. 1063–1068, Sep./Oct. 1996.

[16] A. Rajendran and B. Karthik, "Design and analysis of fuzzy and PI controllers for switched reluctance motor drive," *Mater. Today, Proc.*, vol. 37, no. 2, pp. 1608–1612, 2021, doi: 10.1016/j.matpr.2020.07.166.

[17] S. Paramasivam and R. Arumugam, "Hybrid fuzzy controller for speed control of switched reluctance motor drives," *Energy Convers. Manage.*, vol. 46, nos. 9–10, pp. 1365–1378, 2005.

[18] S.-Y. Wang, F.-Y. Liu, and J.-H. Chou, "Adaptive TSK fuzzy sliding mode control design for switched reluctance motor DTC drive systems with torque sensorless strategy," *Appl. Soft Comput.*, vol. 66, pp. 278–291, May 2018.

[19] M. Divandari, B. Rezaie, and A. R. Noei, "Speed control of switched reluctance motor via fuzzy fast terminal sliding-mode control," *Comput. Electr. Eng.*, vol. 80, Dec. 2019, Art. no. 106472.

[20] H. Cheng, H. Chen, S. Xu, and S. Yang, "Adaptive variable angle control in switched reluctance motor drives for electric vehicle applications," *J. Power Electron.*, vol. 17, no. 6, pp. 1512–1522, 2017.

[21] B. S. Ali, H. M. Hasanien, and Y. Galal, "Speed control of switched reluctance motor using artificial neural network controller," in *Computational Intelligence and Information Technology*, vol. 25. 2011, pp. 6–14.

[22] E. A. Elhay and M. M. Elkholy, "Optimal dynamic and steady-state performance of switched reluctance motor using water cycle algorithm," *IEEJ Trans. Electr. Electron. Eng.*, vol. 13, no. 6, pp. 882–890, Jun. 2018.

[23] H. E. S. A. Ibrahim, M. S. S. Ahmed, and K. M. Awad, "Speed control of switched reluctance motor using genetic algorithm and ant colony based on optimizing PID controller," in *Proc. ITM Web Conf.*, vol. 16, 2018, p. 1001.

[24] M. Yaich and M. Ghariani, "Metaheuristic design and optimization of fuzzy-based SRM speed controller using ant colony algorithm," *J. Eng. Appl. Sci.*, vol. 12, no. 23, pp. 7382–7388, 2017.

[25] J. Deskur, T. Pajchrowski, and K. Zawirski, "Optimal control of current switching angles for high-speed SRM drive," *COMPEL-Int. J. Comput. Math. Electr. Electron. Eng.*, vol. 29, no. 1, pp. 156–172, Jan. 2010.

[26] T. M. P. Dao, Y. N. Wang, and N. K. Nguten, "A novel control approach for switched reluctance motors based on fuzzy logic and particle swarm optimization techniques," *Univ. Politehnica Bucharest Sci. Bull., Series C*, vol. 78, no. 3, p. 12, 2016.

[27] G. A. A. Aziz and M. Amin, "High-precision speed control of four-phase switched reluctance motor fed from asymmetric power converter," *J. Electr. Syst. Inf. Technol.*, vol. 5, no. 3, pp. 300–311, Dec. 2018.

[28] H. Chu, D. Yue, C. Dou, and L. Chu, "Adaptive PI control for consensus of multiagent systems with relative state saturation constraints," *IEEE Trans. Cybern.*, vol. 51, no. 4, pp. 2296–2302, Apr. 2021, doi: 10.1109/TCYB.2019.2954955.

[29] S. Vräna and B. Sulc, "Saturation in engineering simulation," *IFAC Proc. Volumes*, vol. 46, no. 17, pp. 102–107, 2013.

[30] T. L. Chiah and C. L. Hoo, "Hardware simulation of semi-decoupled tuning gain anti-windup PI controllers for motor speed application," in *Proc. AIP Conf.*, 2019, vol. 2137, no. 1, pp. 1–8, doi: 10.1063/1.5120995.

[31] T. C. Tran and J. C. Jung, "Development of anti-windup PI control and bumpless control transfer methodology for feedwater control system," *Ann. Nucl. Energy*, vol. 131, pp. 233–241, Sep. 2019.

[32] P. Sandeep, J. Anjali, and D. Prakash, "Anti-windup fractional order PI^{λ}-PD^{μ} controller design for unstable process: A magnetic levitation study case under actuator saturation," *Arabian J. Sci. Eng.*, vol. 42, no. 12, pp. 5015–5029, 2017.

[33] C. L. Hoo, S. M. Haris, E. C. Y. Chung, and N. A. N. Mohamed, "New integral antiwindup scheme for PI motor speed control," *Asian J. Control*, vol. 17, no. 6, pp. 2115–2132, Nov. 2015.

[34] E. Yousif, C. Kunusch, C. Ocampo-Martinez, and G. Fabricio, "Adaptive PI control with robust variable structure anti-windup strategy for systems with rate-limited actuators: Application to compression systems," *Control Eng. Pract.*, vol. 96, Mar. 2020, Art. no. 104282, doi: 10.1016/j.conengprac.2019.104282.

[35] S. H. Wang, Y. K. Wang, J. H. Hu, X. F. Qin, J. Zheng, and N. Liu, "Anti-windup design for PI-type speed controller based on nonlinear compensation and disturbance suppression," *J. Central South Univ.*, vol. 46, no. 9, pp. 3224–3230, Sep. 2015.

[36] S. C. Song, B. N. Qu, and J. C. Song, "Application of variable gain PI controller in switched reluctance motor," *Miniature Special Motor*, vol. 45, no. 8, pp. 61–64 and 67, 2017.

[37] P. Jan, "Method of mathematical modelling of switched reluctance motors," *Arch. Electr. Eng.*, vol. 53, no. 3, pp. 309–335, 2004.

[38] A. A. Memon and M. M. Shaikh, "Input data for mathematical modeling and numerical simulation of switched reluctance machines," *Data Brief*, vol. 14, pp. 138–142, Oct. 2017.

[39] D. S. Mihic, M. V. Terzic, and S. N. Vukosavic, "A new nonlinear analytical model of the SRM with included multiphase coupling," *IEEE Trans. Energy Convers.*, vol. 32, no. 4, pp. 1322–1334, Dec. 2017.

[40] A. S. Oshaba, E. S. Ali, and S. M. Abd Elazim, "ACO based speed control of SRM fed by photovoltaic system," *Int. J. Electr. Power Energy Syst.*, vol. 67, pp. 529–536, May 2015.

ZIHAN WEI was born in Liaoning, China, in 1998. He received the B.S. degree from Shihezi University, Xinjiang, in 2020, and was recommended to study mechanical engineering at the School of Mechanical and Electrical Engineering, Shihezi University, in the same year.

During his undergraduate studies, he won two national scholarships and has published three articles. His research interests include special motor control, pure electric vehicle drive system control, artificial intelligence, and algorithms and their applications.

MI ZHAO was born in Shihezi, Xinjiang, China, in 1980. She received the B.S., M.S., and Ph.D. degrees from Xidian University, Xi'an, China, in 2002, 2006, and 2009, respectively.

She is currently an Associate Professor with the College of Machinery and Electricity. She has authored or coauthored over 20 publications. She has coauthored the book *Optimal Supervisory Control of Automated Manufacturing Systems*. Her main research interests include modeling, analysis and control of smart grids, and supervisory control of discrete event systems.

XIMU LIU was born in Liaoning, China, in 1997. She received the bachelor's degree from the Northeast Electric Power University, in 2020. She is currently studying for a master's degree in Shihezi University, Xinjiang. During her undergraduate studies, she has published one article. Her research interests include supervisory control of discrete event systems and artificial intelligence algorithms and their applications.

MIN LU received the B.S. degree in control engineering from Xinjiang University, Xinjiang, China, in 2008, and the Ph.D. degree in electrical engineering from the Huazhong University of Science and Technology, Wuhan, China, in 2020. She is currently an Associate Professor with Shihezi University. She mainly engaged in the reliability research of power electronics devices and the wind power generation technology.